Molecular Simulations of Liquid Jet Explosions and Shock Waves Induced by X-Ray Free-Electron Lasers

Leonie Chatzimagas and Jochen S. Hub*
Theoretical Physics and Center for Biophysics, Saarland University, Saarbrücken 66123, Germany

(Received 9 August 2022; revised 8 June 2023; accepted 23 August 2023; published 28 September 2023)

X-ray free-electron lasers (XFELs) produce x-ray pulses with high brilliance and short pulse duration. These properties enable structural investigations of biomolecular nanocrystals, and they allow one to resolve the dynamics of biomolecules down to the femtosecond timescale. Liquid jets are widely used to deliver samples into the XFEL beam. The impact of the x-ray pulse leads to vaporization and explosion of the liquid jet, while the expanding gas triggers the formation of shock wave trains traveling along the jet, which may affect biomolecular samples before they have been probed. Here, we used molecular dynamics simulations to reveal the structural dynamics of shock waves after an x-ray impact. Analysis of the density and temperature in the jet revealed shock waves that form close to the explosion center, travel along the jet with supersonic velocities, and decay exponentially with an attenuation length proportional to the jet diameter. A trailing shock wave formed after the first shock wave, similar to the shock wave trains in experiments. High shock wave velocities in our simulations are compatible with the phenomenon of "fast sound," as emerging at large sound frequencies. Although using purely classical models in the simulations, the resulting explosion geometry and shock wave dynamics closely resemble experimental findings, and they highlight the importance of atomistic details for modeling shock wave attenuation.

DOI: 10.1103/PhysRevLett.131.134003

Introduction.—X-ray free-electron lasers (XFELs) are a source of x-ray radiation that enables novel experiments in the field of structural biology. The high peak brilliance, short pulse duration, and high repetition rates enable resolving the structure of biomolecular nanocrystals, also in a time-resolved manner [1–7]. Liquid jets have been used to deliver the samples rapidly into the beam [8–10]. Upon impact of the x-ray beam, not only the sample is destroyed, but also the segment of the liquid jet exposed to the x-ray pulse is vaporized. The expanding vapor drives the explosion of the liquid jet.

In recent years, several studies analyzed XFEL-induced explosions of liquid droplets or liquid jets [11–16] as well as the relevance of explosions for the design of crystallographic studies. Stan *et al.* used time-resolved imaging to study explosions in droplets and jets, revealing that the expanding vapor launches shock waves traveling across the drops or along the jet [11,12]. In jets, the shock front may split, leading to a sequence of succeeding pressure and density oscillations. These findings have implications for the design of experiments performed at a high x-ray repetition rate, for two reasons [9,13]: First, the gap in the jet formed by the explosion should be replenished before the arrival of the next x-ray pulse, requiring either increased jet velocities or reduced x-ray pulse repetition rates. Second, shock waves traveling backward along the jet may pass the samples before they have been probed. The pressure and density oscillations may perturb the samples leading to lower crystallographic resolution.

The influence of shock waves on biomolecules has been studied both computationally and experimentally. Molecular dynamics (MD) simulations modeling laser-induced shock waves revealed that hemoglobin is compressed during the passage of a shock wave, but the tetrameric structure remained intact [17,18]. Experimentally, comparing crystallographic data of hen egg-white lysozyme (HEWL) microcrystals collected from two successive pulses with 1.1 MHz repetition rate revealed no perturbation of the HEWL microcrystals [9,19,20]. However, since the jet diameter was smaller or approximately equal to the focal spot of the x-ray pulse, no shock waves might have been created according to descriptions by Blaj *et al.* [13]. In contrast, two recent studies found a degradation of diffraction data quality of HEWL and hemoglobin microcrystals as well as structural changes in the hemoglobin microcrystals when probing with an effective pulse repetition rate of 4.5 MHz [10,21]. Additional experimental and computational studies are required to clarify how the experimental design controls the formation and propagation of shock waves, and whether the shock waves affect the biological samples. Here, we used MD simulations to model jet explosions as well as the formation, dynamics, and attenuation of shock waves.

Methods.—We developed a purely classical MD model of the liquid jet and its exposure to an XFEL pulse. We modeled the liquid jet as a water cylinder in vacuum using the all-atom SPC/E water model [22], if not stated otherwise. To test the effect of the water model and the importance of atomic

details, additional simulations were carried out using the all-atom TIP4P/2005 water model [23] or the coarse-grained MARTINI water model [24]. We modeled the explosion of the liquid jet via instantaneous heating of the central jet segment with a Gaussian-shaped temperature distribution by assigning new velocities to the water molecules drawn from the Maxwell-Boltzmann distribution. Since we focused on the shock wave dynamics inside the liquid water, and not on the plasma dynamics, the photoelectric effect and Auger electrons were neglected. We set up simulation systems with jet diameters between 10 nm and 80 nm hit by x-ray beams with intensity profiles with FWHM between 1.5 nm and 12 nm (Table S1 in the Supplemental Material [25]), where the jet diameter was always larger than the FWHM. The jet diameter and the FWHM are at least 1 order of magnitude smaller than the smallest experimental jets [30] and experimental FWHMs [31], respectively. For each system, we carried out 18 to 50 independent simulations in the microcanonical ensemble (Table S1 in the Supplemental Material [25]). To test the role of the jet surface, shock waves in jets were compared to shock waves in a 5 nm × 5 nm × 80 nm water-filled box with periodic boundary conditions (Fig. S1 in the Supplemental Material [25]). We varied the maximum temperature of the initial Gaussian-shaped temperature distribution resulting in maximum temperatures between 5000 K and 100 000 K. Details on the model and simulation parameters are presented in the Supplemental Material [25].

Liquid jet explosion and shock waves.—In the simulations, the impact of the x-ray pulse triggered an explosion of the central jet segment leading to the formation of a gap and, thereby, splitting the jet into two segments [Fig. 1(a) and Fig. S2(a) in the Supplemental Material [25]]. As the gap grew over tens of picoseconds, thin water films formed at the ends of the segments, which later adopted a conical shape, and finally, after several tens of picoseconds, folded back to the jet. Notably, the gap growth dynamics in simulations are in good qualitative agreement with experiments [11] and are compatible with previous theoretical models [11,15] (Fig. S3, Tables S2 and S3, and Supplemental Material [25]). The simulated explosions developed on a by far smaller timescale compared with the experimental jet explosion observed by Stan *et al.* [11] that developed in the microsecond range. The timescale difference is likely a result of the larger experimental jet diameter of 20 μm diameter, which is approximately 3 orders of magnitude larger compared to our MD model. Despite these different length scales and timescales, the jet explosion dynamics in simulations resemble dynamics observed in the experiments.

To analyze shock waves traveling along the jet, we computed the mass density as a function of the axial and radial direction [Figs. 1(b) and S2(b), Supplemental Material [25]]. The data revealed the formation of two density peaks positioned symmetrically around the jet center and close to the explosion site. The peaks traveled

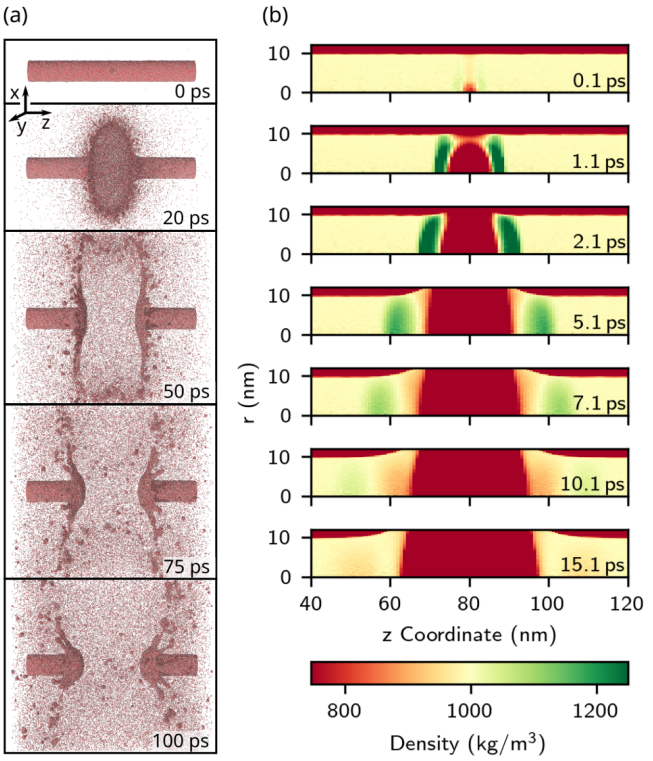

FIG. 1. Simulation of jet explosion with 20 nm diameter induced by a modeled x-ray pulse with 3 nm FWHM. (a) Snapshots of a single simulation. (b) Radial density at 0.1 ps to 15.1 ps after the x-ray impact averaged over 50 independent simulations.

along the jet and decayed to density values slightly below the density of an equilibrated water jet, revealing the rarefaction caused by the shock wave. The density peak was maximized near the jet axis [Fig. 1(b), $r = 0$] but small or even absent at the jet surface ($r \approx 9$ nm). The low densities near the jet surface are explained by the boundary condition at the surface with only the Laplacian pressure owing to surface tension.

Cavitation bubbles, which were detected in experiments close to the explosion site [11,13], were not formed in the simulations, suggesting that the nucleation of cavitation bubbles is a rare event occurring only on larger time and length scales as compared with the scales covered in our simulations (Fig. S4 in the Supplemental Material [25]). Indeed, estimates following Menzl *et al.* suggest for our simulation conditions only a marginal rate of cavitation bubble formation (Supplemental Material [25]) [32].

Averaging the two-dimensional densities along the radial direction yields the time-dependent density as a function of the axial direction z. Here, the density was averaged from the jet axes to a quarter of the jet radius to exclude regions where the shock front is curved and where the density is reduced due to the jet boundary. The density along the axial direction z revealed a second density peak succeeding the first density peak [Fig. 2(a)], as evident from the density evolution at fixed distances from the jet center [Fig. 2(b)].

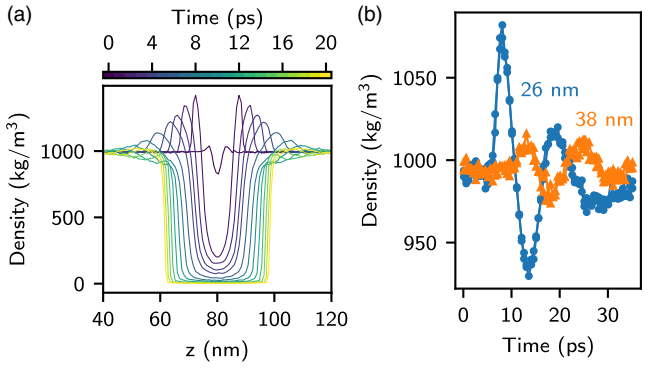

FIG. 2. (a) Time evolution of the density in a water jet with 20 nm diameter after explosion induced by a modeled x-ray pulse with 3 nm FWHM, averaged over 50 simulations. Lines represent the density at time delays of 0.1 to 20.1 ps after x-ray impact (see color bar). (b) Density versus time at fixed distances of 26 nm (blue) or 36 nm (orange) from the jet center.

All the simulations with different combinations of jet diameter and FWHM of the x-ray pulse showed an explosion of the jet and a similar evolution of the densities (Fig. S5 in the Supplemental Material [25]). Hence, despite (i) the approximations underlying the classical models and (ii) the smaller timescales and length scales, the MD simulations reproduce the sequential shock waves observed in previous experiments [11,13].

Attenuation of the shock front.—To analyze the attenuation of the shock front, we determined the height of the first density peak relative to the density of the equilibrated jet. Figure 3(a) presents the height of the peaks for different jet diameters and x-ray pulse widths, plotted versus the propagation distance from the jet center. The attenuation of the density peaks followed an exponential decay, as evident from the linear decay on the semilogarithmic scale. To test the influence of the jet diameter, we scaled the propagated distance of the density peaks by the jet diameter. A linear least-squares fit to the data revealed similar slopes for the peak decay in jets with a different diameter, demonstrating that the decay length is proportional to the jet diameter or, equivalently, to the jet circumference (Table S4 in the Supplemental Material [25]). To test the influence of the jet surface, we furthermore analyzed the density peak attenuation of a shock front in a box with periodic boundary conditions (PBC) and, thus, in absence of a water surface. Notably, the shape of the shock front in the PBC box is characterized by a sharp density peak followed by a gradual decay (Fig. S6 in the Supplemental Material [25]), as is common for shock waves in bulk media [33], and in sharp contrast to the more sinusoidal form of the shock front in the jet [Fig. 2(b)]. The peak height in the PBC box decays exponentially, however, with a decay length that is by far larger as compared to the decay length in the jet [Fig. 3(a), blue circles; Fig. S7(a), Tables S4, and S5 in the Supplemental Material [25]]. Together, these findings suggest that surface effects strongly influence the shock front shape and contribute to energy dissipation.

These results are compatible with experimental observations considering that (i) in experiments, the jets are 3 orders of magnitude larger and the shock front travels further into the jet compared with the simulations, reflecting that decay lengths increase with jet diameter, and (ii) pressure and density are positively correlated, the density evolution of the leading peak agrees with the pressure peak decay calculated from experiments by Blaj *et al.* [13], who suggested that the pressure peaks decay exponentially and that the decay length is approximately proportional to the jet diameter.

Shock wave velocity.—Figure 3(b) presents the peak propagation with time, demonstrating that, after a deceleration in the first 1 to 4 ps, the peaks propagate at a

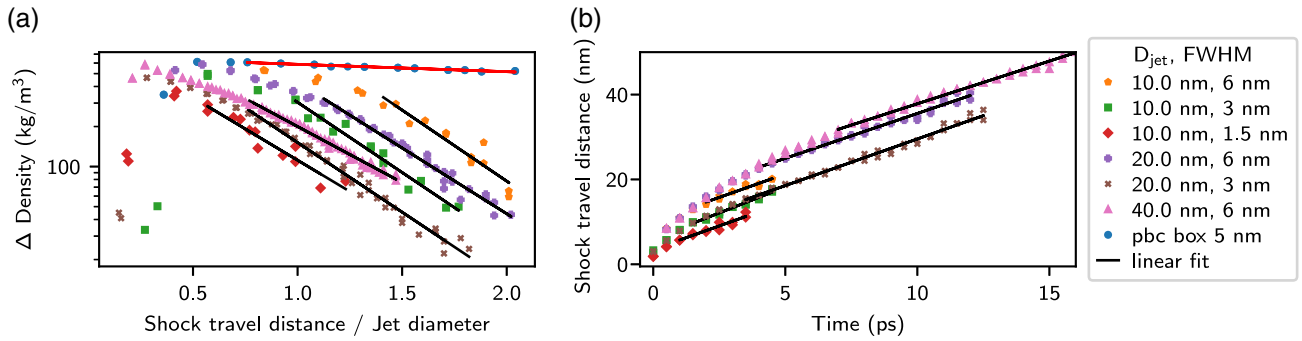

FIG. 3. Shock wave attenuation and propagation. (a) Density peak attenuation of the shock front scaled by the water jet diameter (orange, green, red, purple, brown, and pink symbols). The relative height of the density peaks, Δ Density, attenuates with the propagation distance to the jet center. The linear attenuation on the semilog plot indicates an exponential density decay. The attenuation in the jet approximately scales with the jet diameter. As a comparison the attenuation of a shock wave induced in a box with PBC is shown (blue circles and respective linear fit as red line). The decay length in the PBC box simulation systems is by far larger as compared with the decay length in the jet simulation systems. (b) Propagation of the shock front. The shock propagates with constant, supersonic velocity after a few picoseconds. This velocity is similar among different simulation sets and on average ~2.2 km/s (Table S4 in the Supplemental Material [25]).

constant velocity. The shock wave velocities for all simulation systems are summarized in Table S4 in the Supplemental Material [25], revealing velocities between 2.011 km/s and 2.44 km/s, which are larger than the adiabatic speed of sound in water of ~1.5 km/s.

Critically, in the context of common shock waves [34], the density increase by less than 100 kg/m^3 is too small to rationalize such high shock velocities. Thus, to exclude that the high shock velocities would be an artifact of the SPC/E model, and to investigate the role of the jet geometry on the shock velocities, we obtained shock velocities within the PBC box modeling bulk solvent (Fig. S1 in the Supplemental Material [25]). By instantaneous heating of the central box segment with different peak temperatures between 5000 K and 100 000 K, we generated shock waves with different peak densities. We found that the shock velocities varied between 1.58 km/s and 4.08 km/s and increased with increasing peak densities (Fig. S7 in the Supplemental Material [25]). The relation between peak density and shock velocity was in remarkable agreement with Rice and Walsh [34] (Table S5 columns 4, 5, and 6 in the Supplemental Material [25]), suggesting that (i) the SPC/E model yields reasonably correct shock dynamics and (ii) the high shock velocities in the jet simulations are not explained by the dynamics of common shock waves.

Instead, the high shock velocities beyond the adiabatic speed of sound may be explained by the high-frequency speed of sound, which occurs for sound frequencies larger than a temperature-dependent inverse relaxation time [35–37]. Such "fast sound" was indirectly observed in MD simulations [38,39] and in the excitation spectrum of water [40–42]. The hypothesis of the emergence of high-frequency sound modes in our jet simulations is supported by the facts that (i) shock wave frequencies were ~6×10^{11} Hz for jets with 20 nm diameter [Fig. 2(b)], which is compatible with the experimentally determined frequencies of ~10×10^{11} Hz (or ~4 meV) where the transition to high-frequency sound occurs [41] and (ii) both the shock wave velocities and frequencies decreased with larger jet diameters [13], in line with high-frequency sound modes. Hence, high-frequency speed of sound may manifest in our simulations as shock waves traveling with velocities beyond the adiabatic speed of sound.

Influence of water model and atomic details.—To test the influence of the selected water model, we carried out additional simulations using the four-site TIP4P/2005 model. The results obtained using TIP4P/2005 are in good agreement with the results described above obtained with the three-site SPC/E water model (Figs. S8 and S9 in the Supplemental Material [25]), demonstrating that the choice of the atomistic water model is not critical for modeling shock wave propagation and gap growth.

To test the importance of atomic details for modeling jet explosion and shock wave propagation, we repeated the

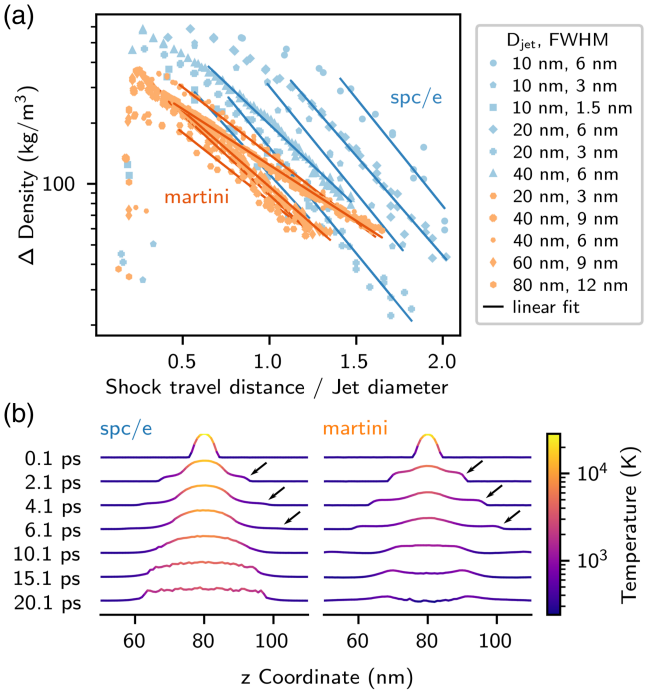

FIG. 4. (a) Influence of atomistic details on density peak attenuation. The density decays over shorter distances when using the atomistic SPC/E model (blue) as compared with using the coarse-grained MARTINI water model (orange). (b) Influence of atomistic details on the time evolution of the temperature in a water jet with 20 nm diameter after explosion induced by a modeled x-ray pulse with 3 nm FWHM, averaged over 20 simulations. Lines represent the temperature at time delays of 0.1 to 20.1 ps after x-ray impact. Height and color of the lines represent the temperature in a logarithmic scale. The energy transported by the shock wave is increased and decays more slowly when using MARTINI (right) as compared with using SPC/E (left). Shock fronts are highlighted by arrows.

simulations with the coarse-grained MARTINI water model [24]. MARTINI describes liquid water as a Lennard-Jones fluid, modeling four molecules by one Lennard-Jones bead. Hence, the MARTINI water model is greatly simplified as it lacks atomic details such as hydrogen bonds, leading to a smoothed potential energy landscape. Despite these simplifications, we observed qualitatively similar explosion and shock wave dynamics compared with simulations using the SPC/E water model (Fig. 4 and Figs. S10 and S11 in the Supplemental Material [25]): the density peaks attenuate exponentially and propagate with a constant velocity after a few picoseconds, and the gap size evolution shows similar trends compared with experimental estimates [11]. However, the simulations reveal a quantitative difference of the shock wave attenuation dynamics compared with SPC/E simulations: While the exponential decay length is still approximately proportional to the jet diameter, the decay length scaled by the jet diameter is larger with MARTINI as compared with SPC/E simulations [Fig. 4(a) and Table S4 in the Supplemental Material [25]]. The difference in the scaled decay length is even more pronounced if the density is

averaged over the entire cross section of the jet (Fig. S12 in the Supplemental Material [25]). Differences between MARTINI and SPC/E simulations are furthermore revealed by the spatial distribution of temperature within the jet. In the MARTINI simulations, the energy transported by the shock wave is increased and the wave decays more slowly as compared with SPC/E simulations [arrows in Fig. 4(b), Figs. S13 and S14 in the Supplemental Material [25]]. Based on the differences in spatial temperature distributions within the jet, we hypothesize that the slower density decay in the MARTINI simulations is a consequence of the smoothed potential energy landscape of the MARTINI model, which may lead to reduced internal friction and, thereby, to slower dissipation of the shock wave energy. Hence, atomistic details are relevant for quantitatively describing the attenuation dynamics of the density peaks.

Conclusion.—We carried out a large set of MD simulations of water jet explosions after impact of an XFEL laser pulse, modeled by a temperature jump of water molecules at the jet center. Despite the approximations underlying our classical simulations, we found good agreement with previous experiments in terms of explosion geometry, shock wave dynamics, and gap growth. These results suggest that photoelectric and Auger effects, which are certainly critical for modeling the explosion at the core of the x-ray impact, are less important for shock wave formation and propagation or for the qualitative dynamics of the gap growth. In the simulations, jet explosion triggered the formation of leading and trailing shock fronts that traveled along the jets. The shocks traveled with velocities larger than expected from the density peak height in the context of common shock waves, which may indicate a manifestation of high-frequency speed of sound in the jet simulations. The shock front attenuated exponentially with a decay length that is (i) proportional to the jet diameter and (ii) shorter than the decay length of a shock in bulk water, suggesting a role of surface effects in dissipation of shock wave energy. Modeling the jet without atomic details led to a slower decay of the shock wave and to an increase of the transported shock energy, likely due to an overly smoothed potential energy landscape of water-water interactions. We expect these insights to be useful for designing experiments at XFELs with high repetition rates.

We thank an anonymous reviewer for pointing us to the phenomenon of "fast sound." This project was supported by the Deutsche Forschungsgemeinschaft (HU 1971/3-1, and INST 256/539-1) and by the German Federal Ministry for Education and Research (Grant No. 16ME0712).

*jochen.hub@uni-saarland.de

[1] H. N. Chapman, X-ray free-electron lasers for the structure and dynamics of macromolecules, Annu. Rev. Biochem. **88**, 35 (2019).

[2] K. Pande, C. D. Hutchison, G. Groenhof, A. Aquila, J. S. Robinson, J. Tenboer, S. Basu, S. Boutet, D. P. DePonte, M. Liang *et al.*, Femtosecond structural dynamics drives the trans/cis isomerization in photoactive yellow protein, Science **352**, 725 (2016).

[3] P. Nogly, T. Weinert, D. James, S. Carbajo, D. Ozerov, A. Furrer, D. Gashi, V. Borin, P. Skopintsev, K. Jaeger *et al.*, Retinal isomerization in bacteriorhodopsin captured by a femtosecond x-ray laser, Science **361**, eaat0094 (2018).

[4] S. Pandey, R. Bean, T. Sato, I. Poudyal, J. Bielecki, J. C. Villarreal, O. Yefanov, V. Mariani, T. A. White, C. Kupitz *et al.*, Time-resolved serial femtosecond crystallography at the European XFEL, Nat. Methods **17**, 73 (2020).

[5] R. Neutze, R. Wouts, D. van der Spoel, E. Weckert, and J. Hajdu, Potential for biomolecular imaging with femtosecond X-ray pulses, Nature (London) **406**, 752 (2000).

[6] P. Roedig, H. M. Ginn, T. Pakendorf, G. Sutton, K. Harlos, T. S. Walter, J. Meyer, P. Fischer, R. Duman, I. Vartiainen *et al.*, High-speed fixed-target serial virus crystallography, Nat. Methods **14**, 805 (2017).

[7] C. Gisriel, J. Coe, R. Letrun, O. M. Yefanov, C. Luna-Chavez, N. E. Stander, S. Lisova, V. Mariani, M. Kuhn, S. Aplin *et al.*, Membrane protein megahertz crystallography at the European XFEL, Nat. Commun. **10**, 5021 (2019).

[8] H. N. Chapman, P. Fromme, A. Barty, T. A. White, R. A. Kirian, A. Aquila, M. S. Hunter, J. Schulz, D. P. DePonte, U. Weierstall *et al.*, Femtosecond X-ray protein nanocrystallography, Nature (London) **470**, 73 (2011).

[9] M. L. Grünbein, J. Bielecki, A. Gorel, M. Stricker, R. Bean, M. Cammarata, K. Dörner, L. Fröhlich, E. Hartmann, S. Hauf *et al.*, Megahertz data collection from protein microcrystals at an X-ray free-electron laser, Nat. Commun. **9**, 3487 (2018).

[10] M. L. Grünbein *et al.*, Observation of shock-induced protein crystal damage during megahertz serial femtosecond crystallography, Phys. Rev. Res. **3**, 013046 (2021).

[11] C. A. Stan, D. Milathianaki, H. Laksmono, R. G. Sierra, T. A. McQueen, M. Messerschmidt, G. J. Williams, J. E. Koglin, T. J. Lane, M. J. Hayes *et al.*, Liquid explosions induced by X-ray laser pulses, Nat. Phys. **12**, 966 (2016).

[12] C. A. Stan, P. R. Willmott, H. A. Stone, J. E. Koglin, M. Liang, A. L. Aquila, J. S. Robinson, K. L. Gumerlock, G. Blaj, R. G. Sierra *et al.*, Negative pressures and spallation in water drops subjected to nanosecond shock waves, J. Phys. Chem. Lett. **7**, 2055 (2016).

[13] G. Blaj, M. Liang, A. L. Aquila, P. R. Willmott, J. E. Koglin, R. G. Sierra, J. S. Robinson, S. Boutet, and C. A. Stan, Generation of high-intensity ultrasound through shock propagation in liquid jets, Phys. Rev. Fluids **4**, 043401 (2019).

[14] D. Ursescu, V. Aleksandrov, D. Matei, I. Dancus, M. D. de Almeida, and C. A. Stan, Generation of shock trains in free liquid jets with a nanosecond green laser, Phys. Rev. Fluids **5**, 123402 (2020).

[15] A. M. Gañán-Calvo, Scaling laws of an exploding liquid column under an intense ultrashort x-ray pulse, Phys. Rev. Lett. **123**, 064501 (2019).

[16] K. R. Beyerlein, H. O. Jönsson, R. Alonso-Mori, A. Aquila, S. Bajt, A. Barty, R. Bean, J. E. Koglin, M. Messerschmidt, D. Ragazzon *et al.*, Ultrafast nonthermal heating of water

initiated by an X-ray Free-Electron Laser, Proc. Natl. Acad. Sci. U.S.A. **115**, 5652 (2018).
[17] F. Wiederschein, Investigation of laser-induced-liquid-beam-ion-desorption (LILBID) with molecular dynamics simulations, Ph.D. thesis, Georg-August-Universität Göttingen, 2009.
[18] E. Vöhringer-Martinez, Dynamics, ionization and charge separation in superheated metastable water, Ph.D. thesis, Georg-August-Universität Göttingen, 2008.
[19] M. O. Wiedorn, D. Oberthür, R. Bean, R. Schubert, N. Werner, B. Abbey, M. Aepfelbacher, L. Adriano, A. Allahgholi, N. Al-Qudami *et al.*, Megahertz serial crystallography, Nat. Commun. **9**, 4025 (2018).
[20] O. Yefanov, D. Oberthür, R. Bean, M. O. Wiedorn, J. Knoska, G. Pena, S. Awel, L. Gumprecht, M. Domaracky, I. Sarrou *et al.*, Evaluation of serial crystallographic structure determination within megahertz pulse trains, Struct. Dyn. **6**, 064702 (2019).
[21] M. L. Grünbein, A. Gorel, L. Foucar, S. Carbajo, W. Colocho, S. Gilevich, E. Hartmann, M. Hilpert, M. Hunter, M. Kloos *et al.*, Effect of X-ray free-electron laser-induced shockwaves on haemoglobin microcrystals delivered in a liquid jet, Nat. Commun. **12**, 1 (2021).
[22] S. Chatterjee, P. G. Debenedetti, F. H. Stillinger, and R. M. Lynden-Bell, A computational investigation of thermodynamics, structure, dynamics and solvation behavior in modified water models, J. Chem. Phys. **128**, 124511 (2008).
[23] J. L. Abascal and C. Vega, A general purpose model for the condensed phases of water: TIP4P/2005, J. Chem. Phys. **123**, 234505 (2005).
[24] S. J. Marrink, H. J. Risselada, S. Yefimov, D. P. Tieleman, and A. H. De Vries, The MARTINI force field: coarse grained model for biomolecular simulations, J. Phys. Chem. B **111**, 7812 (2007).
[25] See Supplemental Material at http://link.aps.org/supplemental/10.1103/PhysRevLett.131.134003 for Figs. S1–S5, Tables S1–S2, computational details, models of gap growth, and Refs. [26–29].
[26] S. Miyamoto and P. A. Kollman, Settle: An analytical version of the SHAKE and RATTLE algorithm for rigid water models, J. Comput. Chem. **13**, 952 (1992).
[27] G. Bussi, D. Donadio, and M. Parrinello, Canonical sampling through velocity rescaling, J. Chem. Phys. **126**, 014101 (2007).
[28] D. Van Der Spoel and P. J. van Maaren, The origin of layer structure artifacts in simulations of liquid water, J. Chem. Theory Comput. **2**, 1 (2006).
[29] T. Darden, D. York, and L. Pedersen, Particle mesh Ewald: An $N \log(N)$ method for Ewald sums in large systems, J. Chem. Phys. **98**, 10089 (1993).
[30] M. L. Grünbein and G. Nass Kovacs, Sample delivery for serial crystallography at free-electron lasers and synchrotrons, Acta Crystallogr. Sect. D **75**, 178 (2019).
[31] H. Mimura, H. Yumoto, S. Matsuyama, T. Koyama, K. Tono, Y. Inubushi, T. Togashi, T. Sato, J. Kim, R. Fukui *et al.*, Generation of $10^{20}\,\mathrm{W\,cm^{-2}}$ hard X-ray laser pulses with two-stage reflective focusing system, Nat. Commun. **5**, 3539 (2014).
[32] G. Menzl, M. A. Gonzalez, P. Geiger, F. Caupin, J. L. Abascal, C. Valeriani, and C. Dellago, Molecular mechanism for cavitation in water under tension, Proc. Natl. Acad. Sci. U.S.A. **113**, 13582 (2016).
[33] N. Abdul-Karim, C. S. Blackman, P. P. Gill, E. M. M. Wingstedt, and B. A. P. Reif, Post-blast explosive residue—a review of formation and dispersion theories and experimental research, RSC Adv. **4**, 54354 (2014).
[34] M. H. Rice and J. M. Walsh, Equation of State of Water to 250 Kilobars, J. Chem. Phys. **26**, 824 (1957).
[35] A. Cunsolo, G. Ruocco, F. Sette, C. Masciovecchio, A. Mermet, G. Monaco, M. Sampoli, and R. Verbeni, Experimental determination of the structural relaxation in liquid water, Phys. Rev. Lett. **82**, 775 (1999).
[36] A. Cunsolo, G. Ruocco, F. Sette, C. Masciovecchio, A. Mermet, G. Monaco, M. Sampoli, and R. Verbeni, Experimental determination of the structural relaxation in liquid water, Phys. Rev. Lett. **82**, 2810 (1999).
[37] G. Ruocco and F. Sette, The history of the "fast sound" in liquid water, Condens. Matter Phys. **11**, 29 (2008).
[38] A. Rahman and F. H. Stillinger, Propagation of sound in water. A molecular-dynamics study, Phys. Rev. A **10**, 368 (1974).
[39] F. Sciortino and S. Sastry, Sound propagation in liquid water: The puzzle continues, J. Chem. Phys. **100**, 3881 (1994).
[40] F. Sette, G. Ruocco, M. Krisch, U. Bergmann, C. Masciovecchio, V. Mazzacurati, G. Signorelli, and R. Verbeni, Collective dynamics in water by high energy resolution inelastic x-ray scattering, Phys. Rev. Lett. **75**, 850 (1995).
[41] F. Sette, G. Ruocco, M. Krisch, C. Masciovecchio, R. Verbeni, and U. Bergmann, Transition from normal to fast sound in liquid water, Phys. Rev. Lett. **77**, 83 (1996).
[42] S. C. Santucci, D. Fioretto, L. Comez, A. Gessini, and C. Masciovecchio, Is there any fast sound in water?, Phys. Rev. Lett. **97**, 225701 (2006).